Supporting Information for

Single-Atom Catalysis Enabled by High-Energy Metastable Structures

Zhaoming Xia, Yue Yin, Jun Li, Hai Xiao*

Department of Chemistry and Key Laboratory of Organic Optoelectronics & Molecular Engineering of Ministry of Education, Tsinghua University, Beijing 100084, China

Additional computational details

The surface structure of CeO_2(110) is shown in **Figure S1**, and we consider the Ce site, O site, O bridging site, and 4-fold hollow site labeled in **Figure S1** for accommodating M_1. This results in three types of M_1/CeO_2 SACs: 1) the M atom substituting the Ce site[1-2], labelled as M_{subCe} (**Figure S2**); 2) the M atom substituting the O site[3], labelled as M_{subO} (**Figure S3**); 3) the M atom supported on the O bridging site or the 4-fold hollow site[4-7], labelled as $M_{support}$ (**Figure S4**). In addition, when SACs are exposed to an oxidizing or reducing environment, the surface O stoichiometry may vary. Thus, additional types are derived from M_{subCe} and $M_{support}$ by adding or removing O atoms on the surface, which are labeled as $M_{subCe\text{-}O}$ (**Figure S5**), $M_{subCe+O}$ (**Figure S6**), $M_{suport\text{-}O}$ (**Figure S7**), $M_{suport+O}$ (**Figure S8**), respectively. The M_{subO} type requires the reducing environment to create the O vacancy (O_v) for hosting M_1, and it turns into the M_{subCe} or $M_{support}$ type under the oxidizing environment, so there is no new type derived from it.

The Gibbs free energy corrections (including both the enthalpic and entropic terms) of gas phase molecules and surface-adsorbed species were calculated with the ideal-gas approximation and the harmonic approximation for the vibrational degrees of freedom using the thermochemistry modules of the Atomic Simulation Environment (ASE).

The formation energy (ΔG_f) of SAC is calculated using the following equation,

$$\Delta G_f = E_{M-CeO_2-x\mathrm{Cev}-y\mathrm{Ov}} - E_{CeO_2} - E_{M-bulk} + x\mu_{Ce} + y\mu_O$$

where $E_{M-CeO_2-x\mathrm{Cev}-y\mathrm{Ov}}$ is the energy of SAC; x is the number of Ce vacancies; y is the number of O_v (if $y < 0$, $-y$ is the number of extra O atoms); E_{CeO_2} is the energy of pristine CeO_2 surface; E_{M-bulk} is the energy per atom of the metal bulk; μ_O is the chemical potential of O, and μ_{Ce} is the chemical potential of Ce in CeO_2, calculated as

$$\mu_{Ce} = E_{CeO_2-bulk} - 2\mu_O$$

where E_{CeO_2-bulk} is the energy per CeO_2 unit of CeO_2 bulk.

The μ_O-dependent ΔG_f's for all SACs are shown in **Figure S9**. The most stable phase changes significantly with μ_O for all the SACs, and this indicates that the local structure of SAC under reaction conditions can be quite different from the result of *ex situ* characterization. In order to correspond to the real reaction conditions, μ_O is mapped into a function of temperature and partial pressure of a typical gas in the reaction environment. We consider two typical reaction conditions,

1. In the oxidative condition, we take the O_2 gas as the representative, and

$$\mu_O = \frac{1}{2}G_{O_2}$$

where G_{O_2} is the Gibs free energy of O_2 gas.

2. In the reductive condition, we take the H_2 gas as the representative, and μ_O is defined as follows,[8]

$$\mu_O = G_{H_2O} - G_{H_2}$$

where G_{H_2O} and G_{H_2} are the Gibs free energies of water vapor and H_2 gas, respectively.

Based on the ΔG_f's of all types of structures for each SAC, we calculate the phase diagrams of SACs under different reaction conditions (**Figures S10-S12**), according to the Boltzmann distribution.

Supplementary Note on the partial pressure of HCOOH

In the experiments, alkali solutions were widely used to absorb HCOOH to achieve large TOFs, and this results in extremely small concentrations of HCOOH in the solution. If we assume that there is already 0.1 M HCOOH produced and absorbed in the alkaline solution with a pH of 14, based on the pKa (3.74) of HCOOH, the concentration of HCOOH ([HCOOH]) is only $10^{-11.26}$ M ([$HCOO^-$] is approximately 10^{-1} M). Then, according to the Henry's law constant of HCOOH in water solution (8.9×10^3 M/bar, taken from *J. Atmos. Chem.* **1996**, *24*, 113-119), the vapor pressure of HCOOH is 0.6×10^{-15} bar. In our microkinetic modeling, the partial pressure of HCOOH was thus set to 10^{-15} bar in accordance with the experiments' conditions.

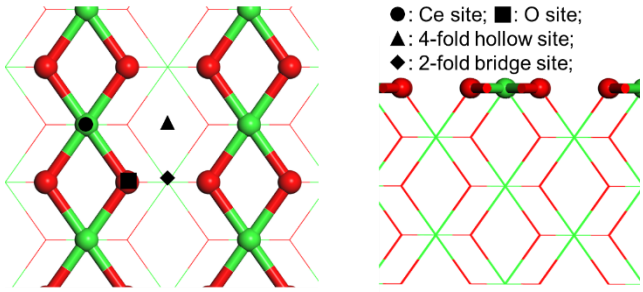

Figure S1. Surface structure of CeO_2(110) and the sites considered in this study. Left: top view; right: side view.

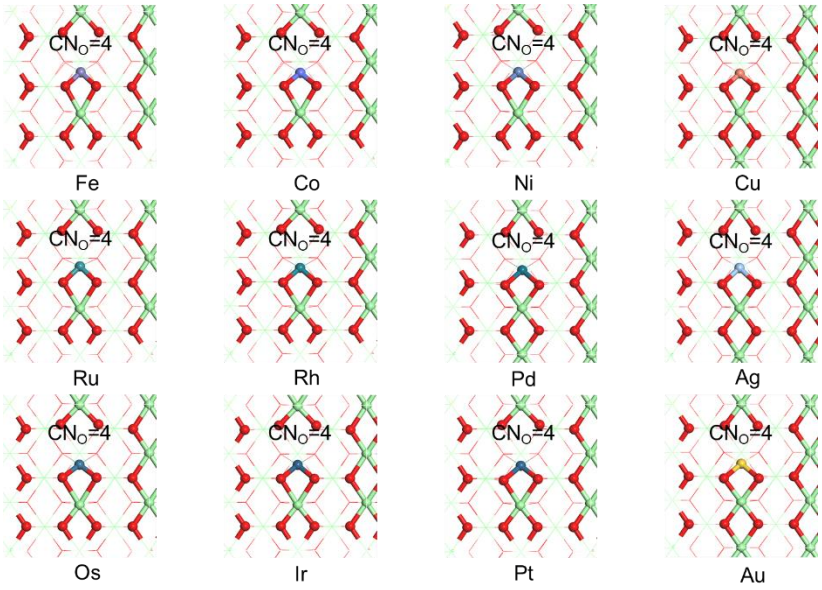

Figure S2. Optimized structures of the M_{subCe} type of M_1/CeO_2 SACs. Note that the M_1 substituting Ce is relaxed to a more stable 4-fold coordinated configuration different from that of the original Ce.

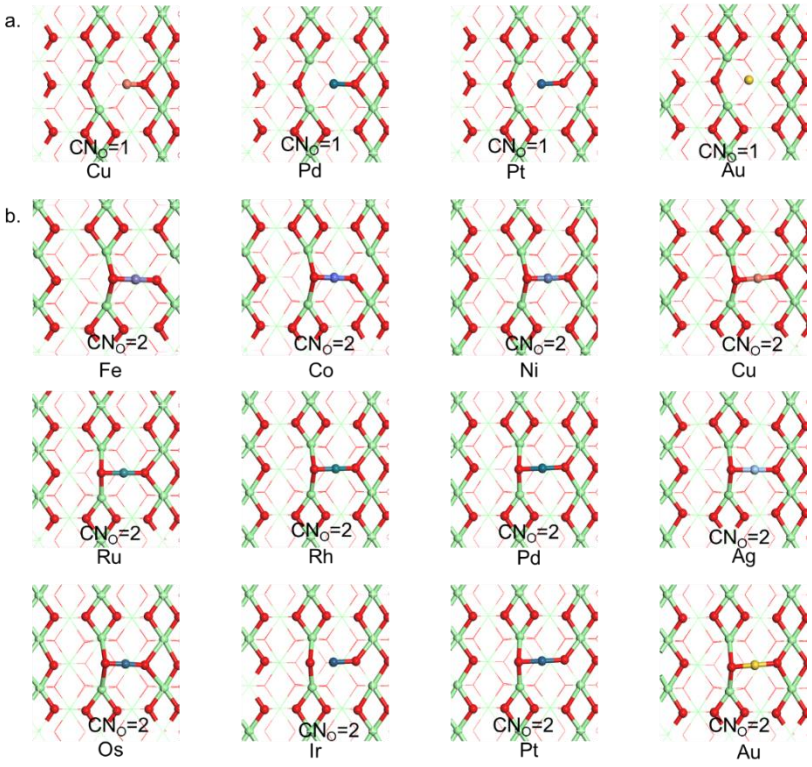

Figure S3. Optimized structures of the M_{subO} type of M_1/CeO_2 SACs. a: M_{subO-1}; b: M_{subO-2}. Only Cu, Pd, Pt and Au can be relaxed into M_{subO-1} configuration.

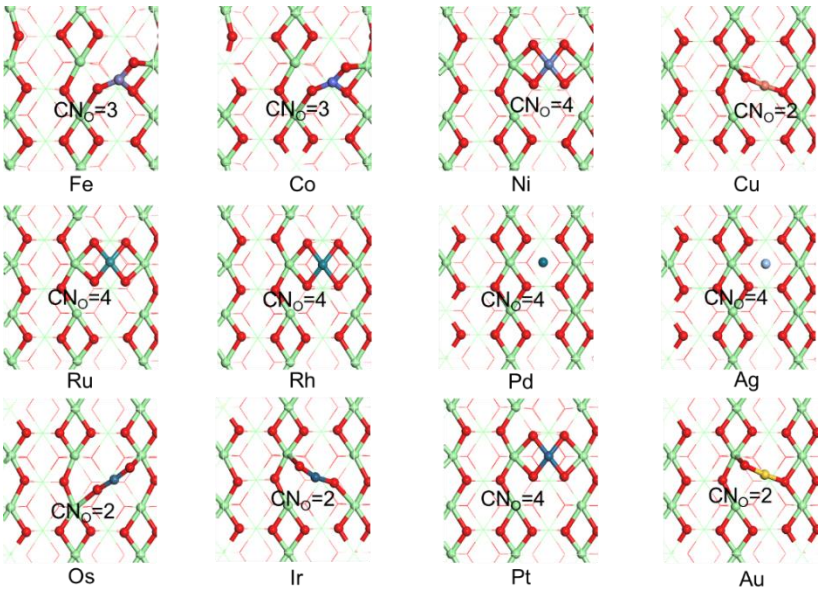

Figure S4. Optimized structures of the $M_{support}$ type of M_1/CeO_2 SACs. For Ni, Ru, Rh, Pd, Ag, and Pt, the M_1 prefers to adsorb at the 4-fold hollow site, while for Cu, Os, Ir, and Au, the M_1 prefers to adsorb at the 2-fold bridge site. For Fe and Co, the M_1 prefers to adsorb at the 4-fold hollow site but is relaxed to a more stable distorted 3-fold coordinated configuration.

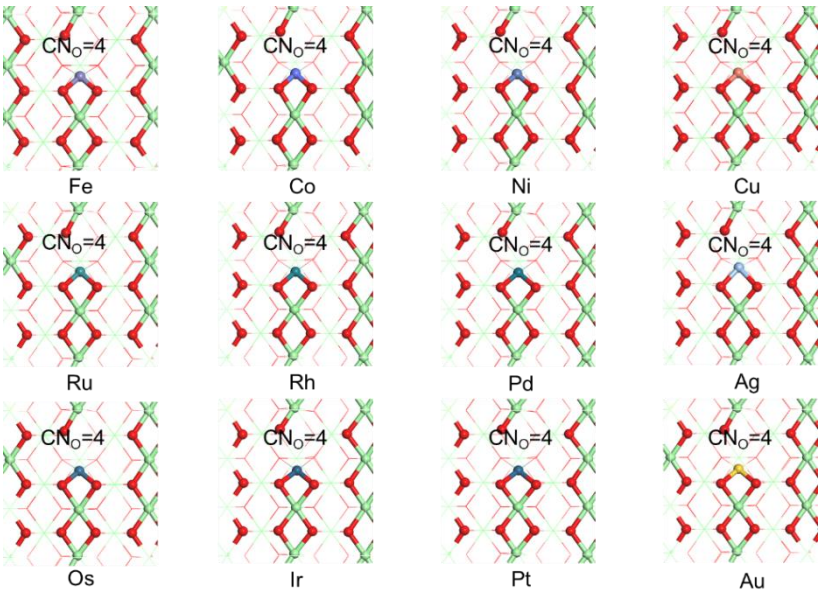

Figure S5. Optimized structures of the $M_{subCe\text{-}O}$ type of M_1/CeO_2 SACs.

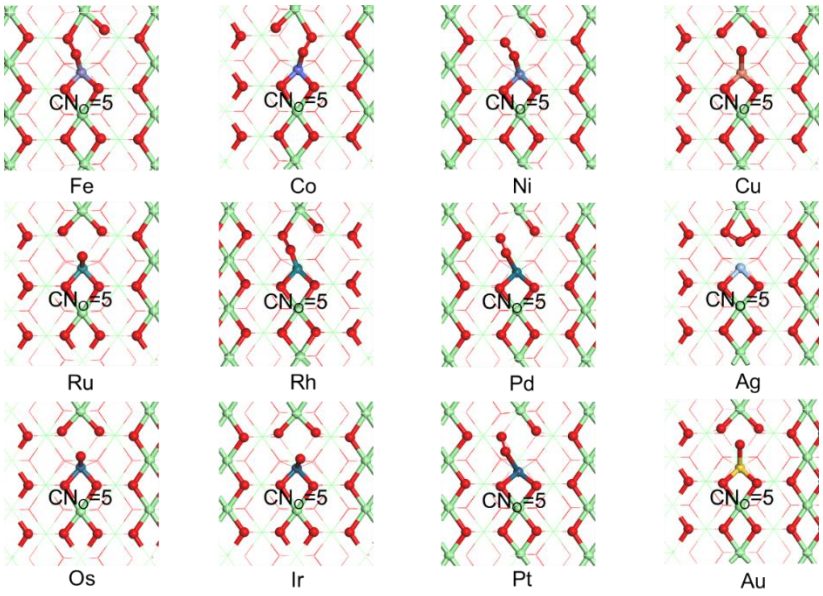

Figure S6. Optimized structures of the $M_{subCe+O}$ type of M_1/CeO_2 SACs.

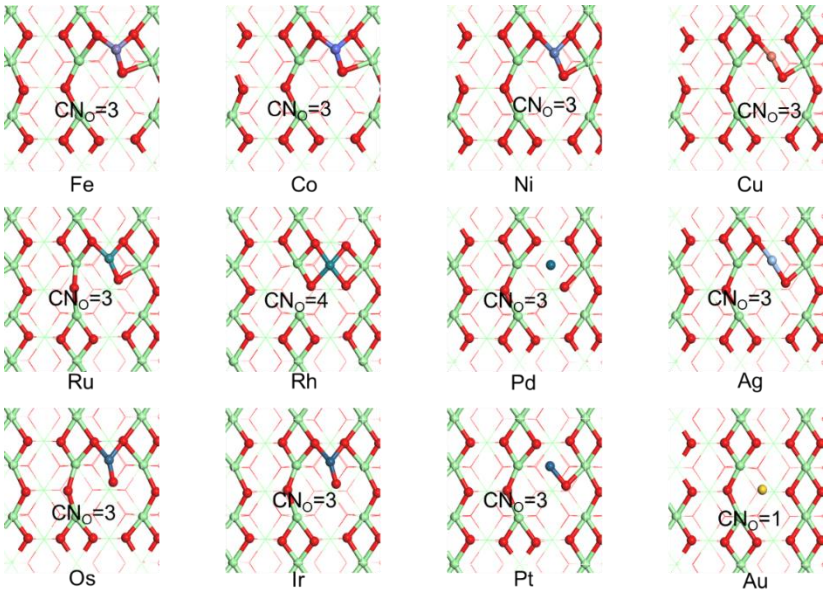

Figure S7. Optimized structures of the $M_{suport\text{-}O}$ type of M_1/CeO_2 SACs. Among all the $M_{suport\text{-}O}$ structures, Au_1 is relaxed to the same local structure as $M_{subO\text{-}1}$, while all the other M_1's are optimized to a new type of local structures. Note that only the O atoms near M_1 in M_{suport} are removed to model the local structure of active site in reductive environment, even though the formation energy of O_v at further sites may be lower, because the formation of O_v far from M_1 does not change the local coordination of M_1.

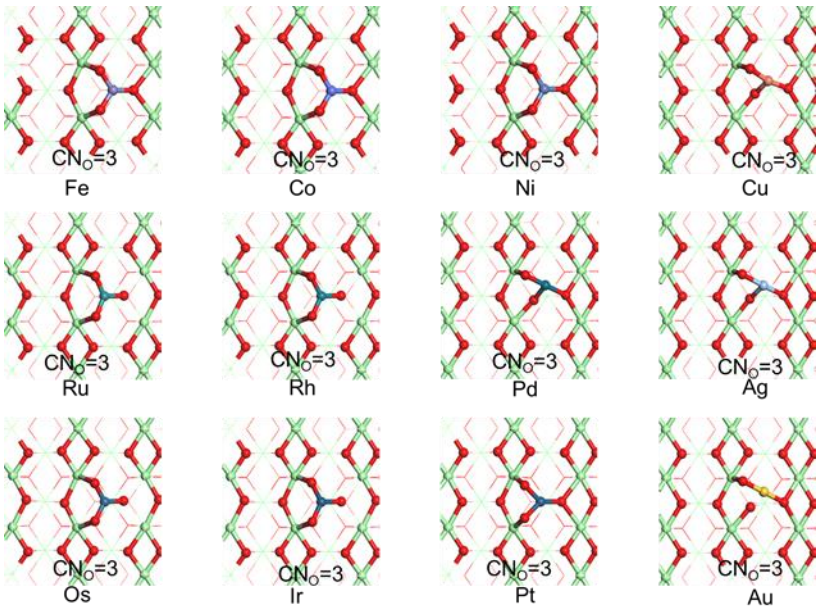

Figure S8. Optimized structures of the $M_{support+O}$ type of M_1/CeO_2 SACs.

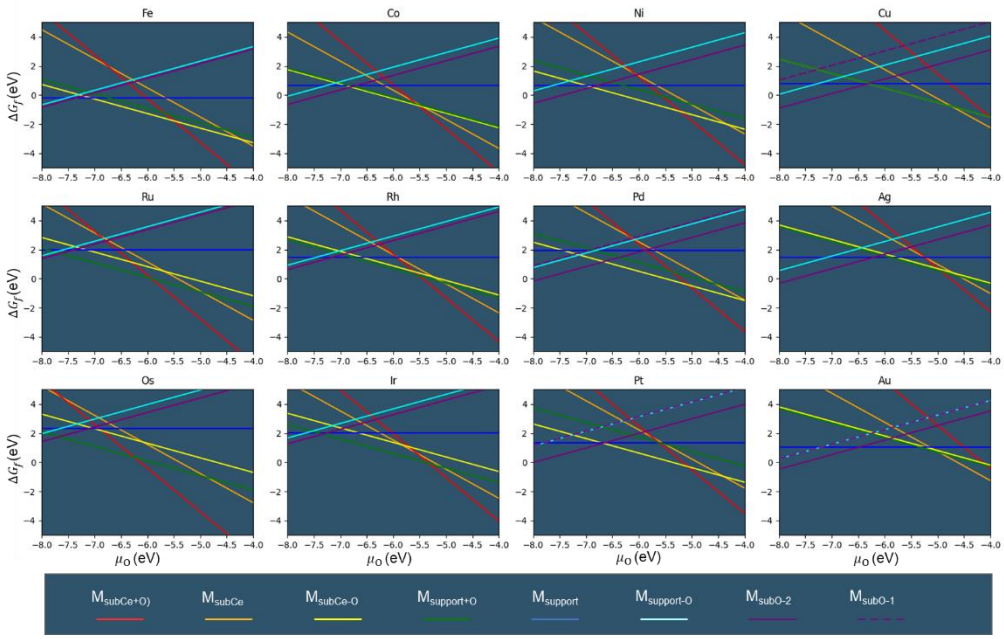

Figure S9. The μ_O-dependent formation energies of all SACs.

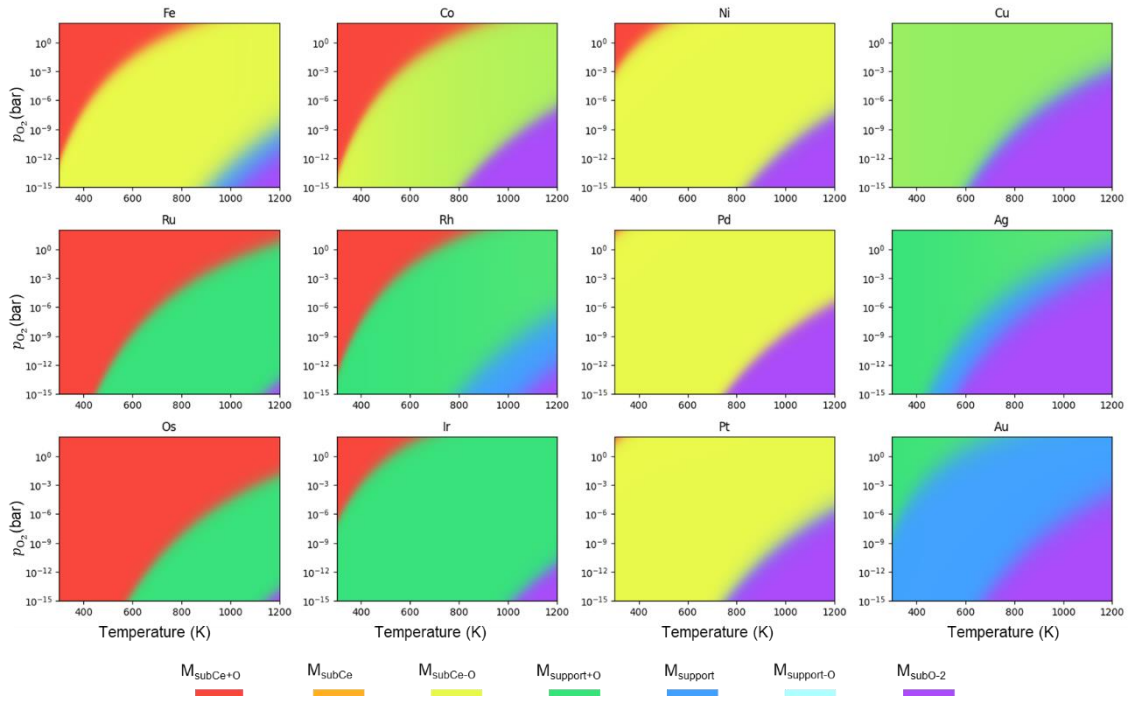

Figure S10. Phase diagrams of M_1/CeO_2 SACs in oxidative conditions. Each phase is represented by a distinct RGB color (RGB_i), and the color of each point in the phase diagram is defined as the overlay of RGB_i weighted by the proportion of each phase. Therefore, the yellow and green color mixing area in the phase diagram of Co SAC indicates a coexistence of $Co_{subCe-O}$ and $Co_{suport+O}$ types of structures, this is because their formation energies are close, with an energy difference of only 0.07 eV.

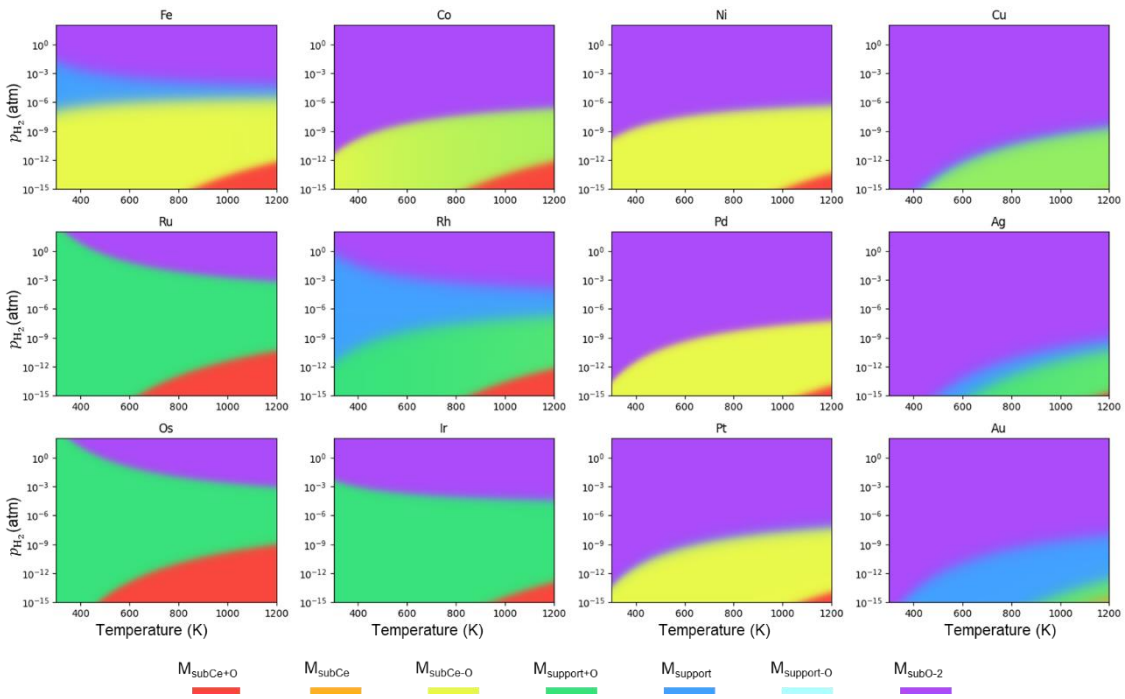

Figure S11.Phase diagrams of M_1/CeO_2 SACs in reductive conditions. The partial pressure of water vapor is 10^{-4} bar. Each phase is represented by a distinct RGB color (RGB_i), and the color of each point in the phase diagram is defined as the overlay of RGB_i weighted by the proportion of each phase. Therefore, the yellow and green color mixing area in the phase diagram of Co SAC indicates a coexistence of $Co_{subCe-O}$ and $Co_{suport+O}$ types of structures, this is because their formation energies are close, with an energy difference of only 0.07 eV.

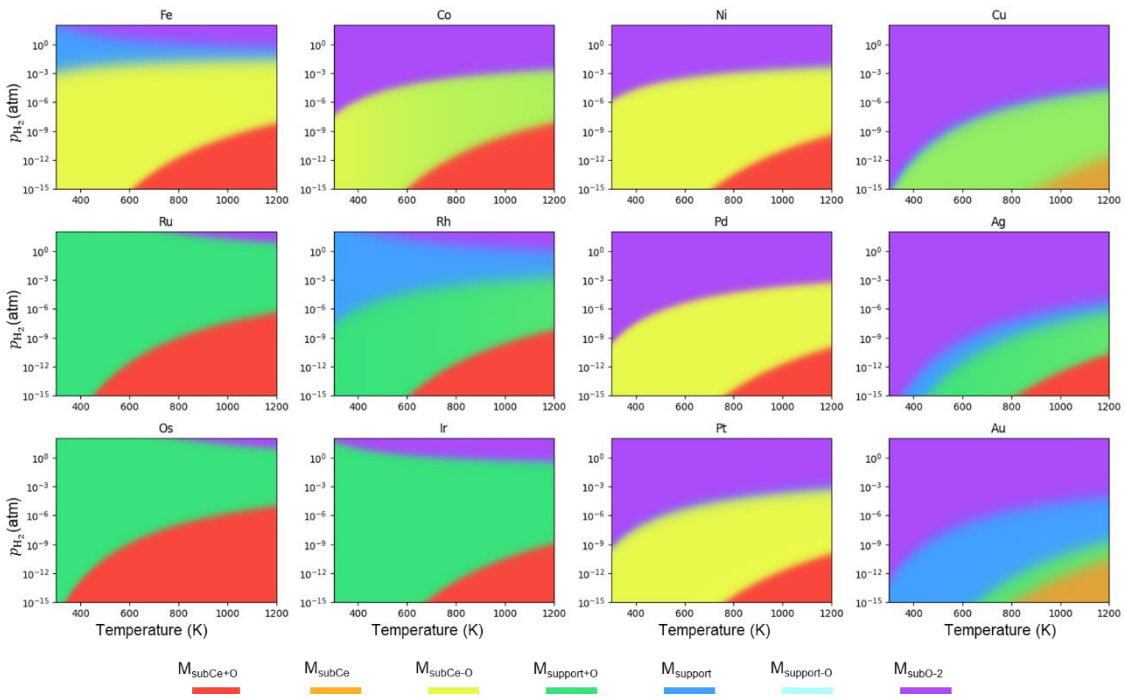

Figure S12. Phase diagrams of M_1/CeO_2 SACs in reductive conditions. The partial pressure of water vapor is 1 bar. Each phase is represented by a distinct RGB color (RGB_i), and the color of each point in the phase diagram is defined as the overlay of RGB_i weighted by the proportion of each phase. Therefore, the yellow and green color mixing area in the phase diagram of Co SAC indicates a coexistence of $Co_{subCe-O}$ and $Co_{suport+O}$ types of structures, this is because their formation energies are close, with an energy difference of only 0.07 eV.

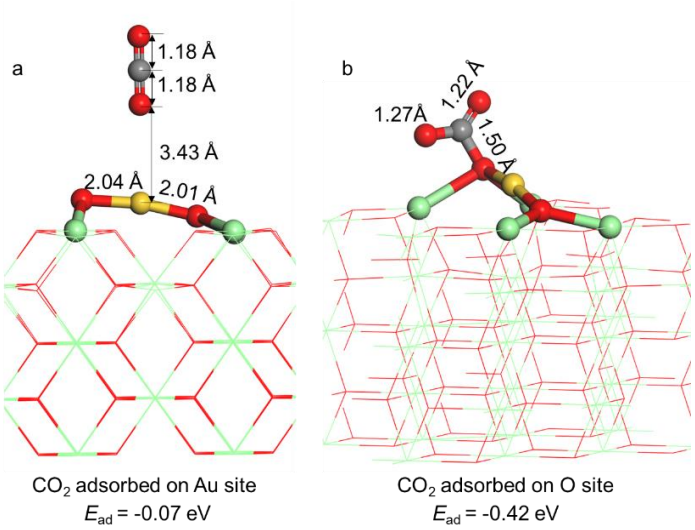

Figure S13. CO_2 adsorption modes on the LES. (a) Physisorption of CO_2 on the positively charged Au site. (b) Chemisorption of CO_2 on the surface O site. E_{ad} is defined as $E_{tot} - E_{slab} - E_{CO2}$, where E_{tot} is the energy of adsorbed structure, E_{slab} is the energy of the clean surface, E_{CO2} is the energy of CO_2 gas molecule.

The C-O bond length of CO_2 in (a) is the same as that of gas phase CO_2, so the CO_2 in (a) is not activated. Besides, the CO_2 adsorption mode in (a) is higher in energy than that in (b). Thus, (a) is ignored in the following consideration.

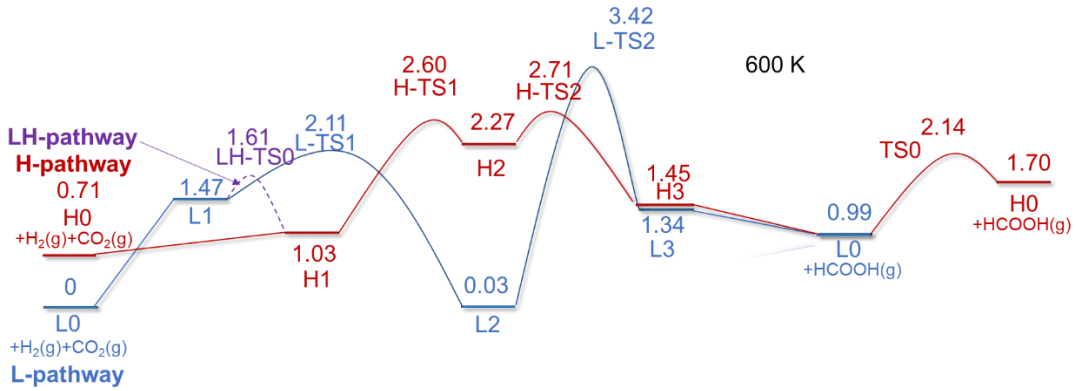

Figure S14. Free energy profiles (in eV) of CO_2HR on Au_1/CeO_2 SAC at 600 K.

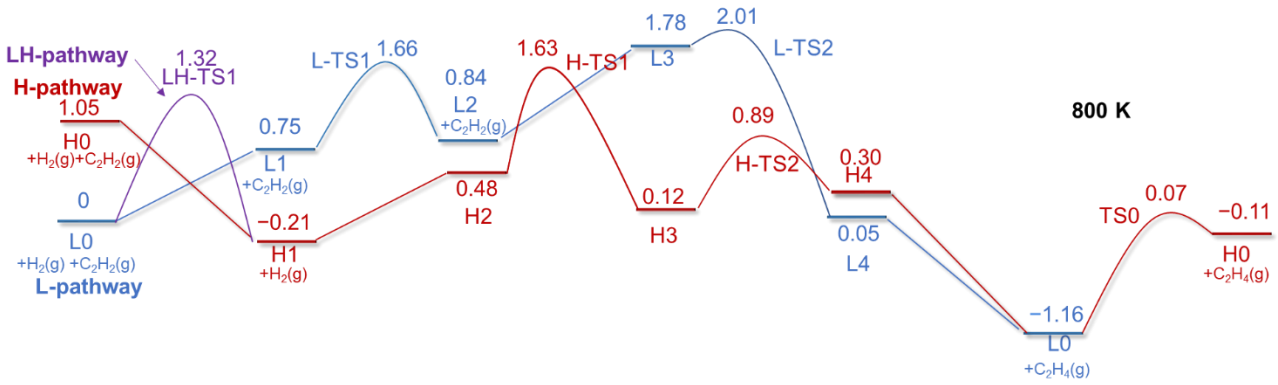

Figure S15. Free energy profiles (in eV) of SHA on Pt_1/CeO_2 SAC at 800 K.

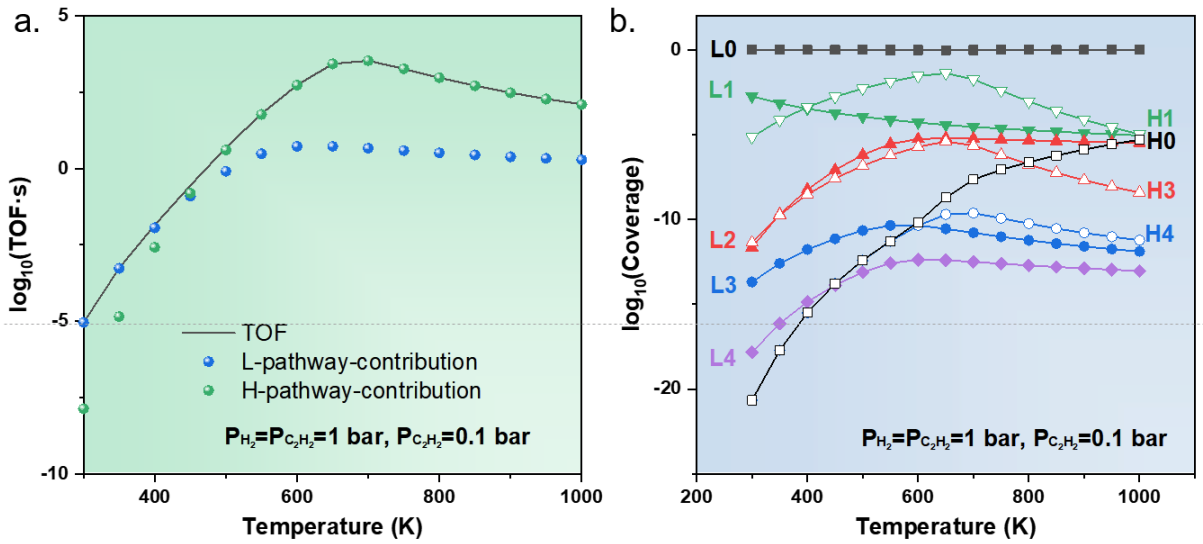

Figure S16. Calculated (a) TOF and (b) coverages of states as functions of temperature for the SHA on Pt_1/CeO_2 SAC, assuming that there is no LH-pathway.

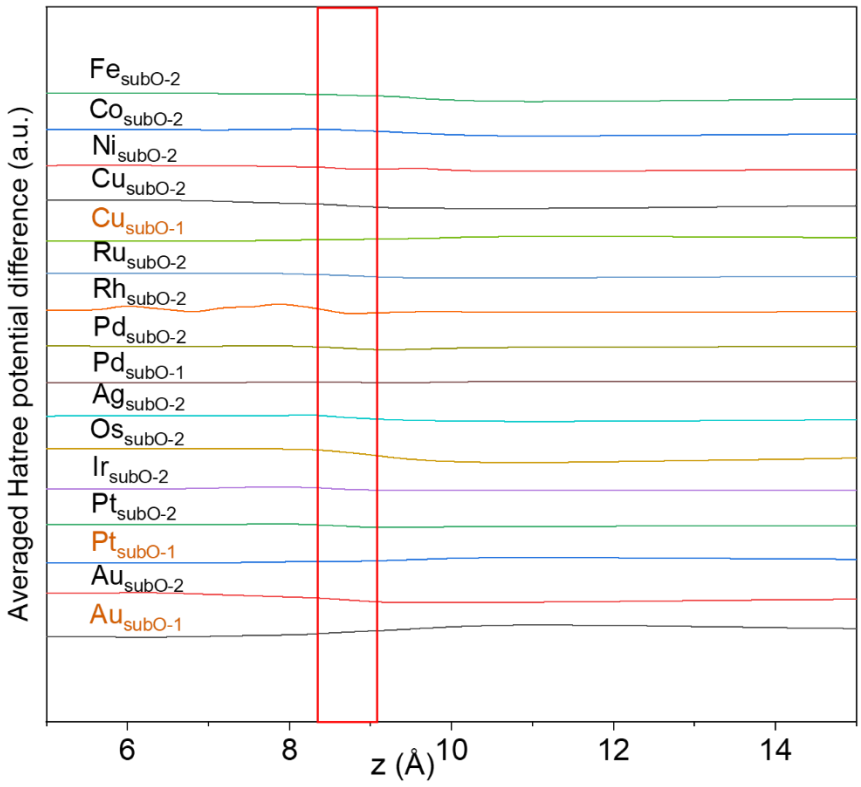

Figure S17. Hartree potential differences projected onto the *z*-axis. The Hartree potential difference (ΔV_H) is defined as $\Delta V_H = V_{H\text{-}SA/support} - V_{H\text{-}support} - V_{H\text{-}SA}$, where $V_{H\text{-}SA/support}$, $V_{H\text{-}support}$, $V_{H\text{-}support}$ are the Hartree potentials of SAC, isolated support, and the isolated single-atom, respectively. In general, ΔV_H can be regarded as a measure of the change in the interface local potential induced by the metal adatom. The increase of ΔV_H along the *z*-direction indicates the charge transfer from the support to the metal adatom, and the decrease of ΔV_H implies the opposite.

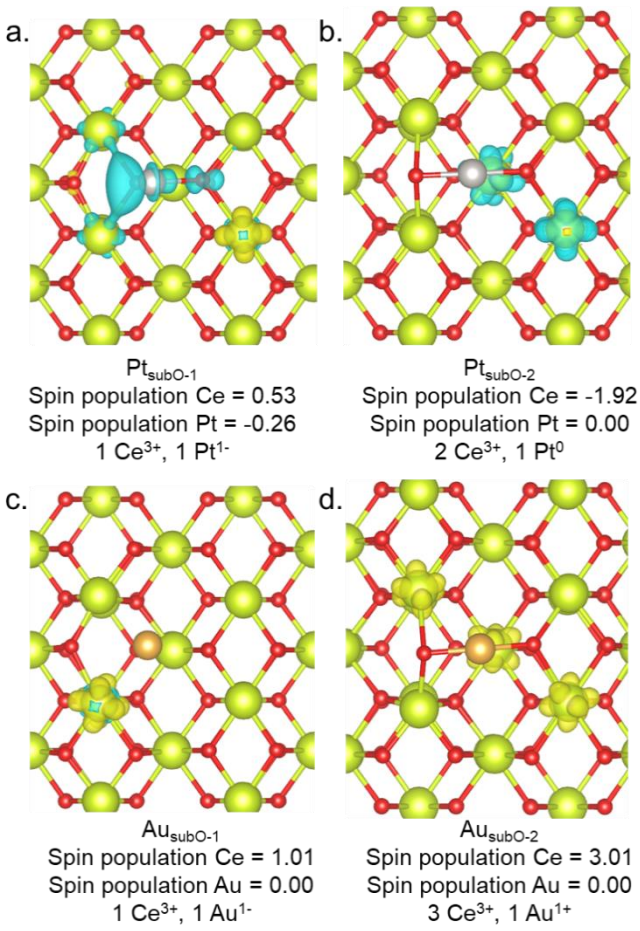

Figure S18. Spin density isosurfaces at 0.005 e/Bohr^3. The yellow and cyan isosurfaces represent the alpha and beta spins, respectively. The unpaired electron in Ce 4*f* orbital is clearly displayed, which can be used to identify the Ce^{3+} ions. One O_v will leave two extra electrons in the CeO_2 support, which create two Ce^{3+}. Extra electrons transferred from M_1 also create Ce^{3+} ions. Thus, the oxidation state of M_1 formally equals to $n(Ce^{3+}) - 2$, where $n(Ce^{3+})$ is the total number of Ce^{3+} ions.

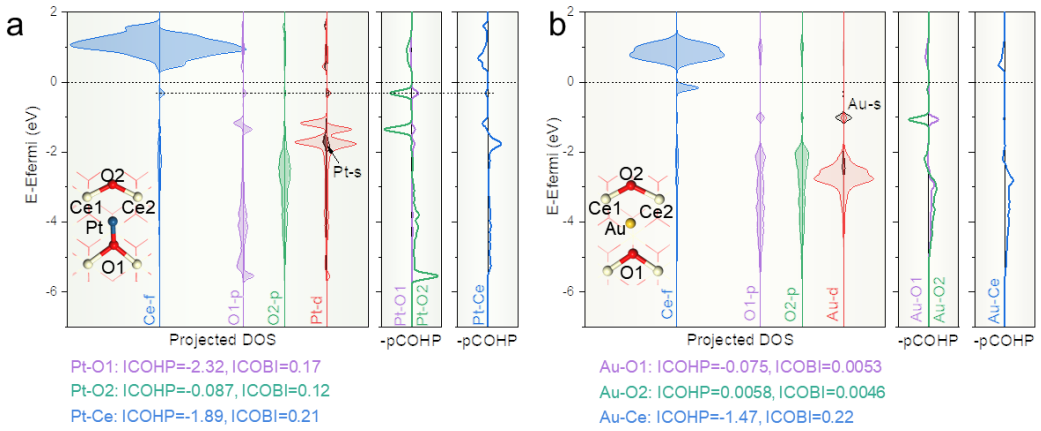

Figure S19. Projected densities of states (pDOSs) and projected crystal orbital Hamilton populations (pCOHPs) of the negatively charged (a) Pt_1/CeO_2 and (b) Au_1/CeO_2 SACs.

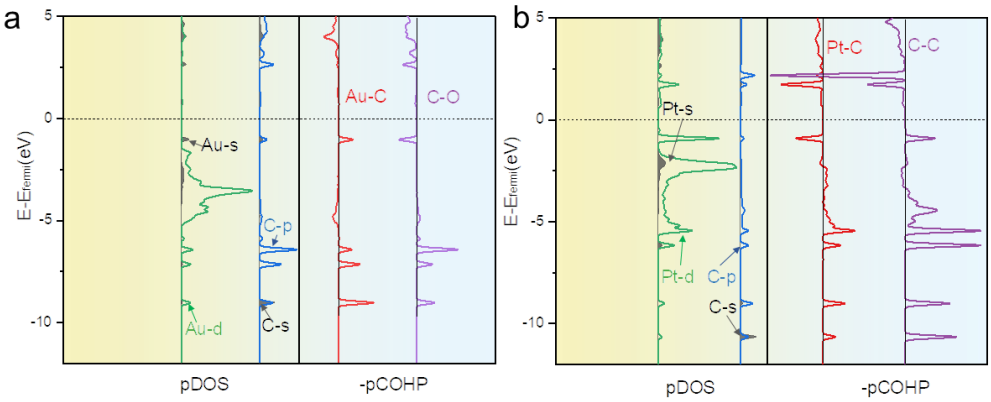

Figure S20. The pDOSs and pCOHPs of (a) CO_2 adsorption on Au_1/CeO_2 and (b) C_2H_2 adsorption on Pt_1/CeO_2.

Table S1. Relative energy of each state.

	Most stable state M_{subO-2}	Transition state (from M_{subO-2} to M_{subO-1})	Metastable state M_{subO-1}
Cu	0 eV	1.96 eV	1.93 eV
Pd	0 eV	1.17 eV	1.07 eV
Pt	0 eV	1.23 eV	1.05 eV
Au	0 eV	1.15 eV	0.71 eV

Table S2. The 1*s* core level shift and oxidative state (OS) of M in each model.

Oxidation state		−1	0	+1	+2	M_{subO-1}	M_{subO-2}
Reference		MCs	M	MCl	MO		
Relative 1*s* core level (eV)	Pt	−0.72	0.00	1.39	3.06	−0.20 (−1)	0.0007 (0)
	Au	−1.68	0.00	1.46	2.68	−0.33 (−1)	1.08 (+1)

The oxidation states of M in MCs, M, MCl, and MO gas phase molecules are formally −1, 0, +1, and +2, respectively. The relative 1*s* core level is defined as the 1*s* core level of M in each model referenced to that in the gas phase M atom. The core level is corrected by putting an Ar atom in the unit cell to make sure that the energy difference between the 1*s* level of Ar and vacuum level is constant. The oxidation state (number in parenthesis) of M_1 in the SAC is determined by considering the sign of core level shift first and then its absolute value.

References

1. Tang, Y.; Wang, Y.-G.; Li, J., Theoretical Investigations of Pt1@CeO2 Single-Atom Catalyst for CO Oxidation. *J. Phys. Chem. C* **2017,** *121* (21), 11281-11289.
2. Zhao, S.; Kang, D.; Liu, Y.; Wen, Y.; Xie, X.; Yi, H.; Tang, X., Spontaneous Formation of Asymmetric Oxygen Vacancies in Transition-Metal-Doped CeO2 Nanorods with Improved Activity for Carbonyl Sulfide Hydrolysis. *ACS Catal.* **2020,** *10* (20), 11739-11750.
3. Chen, Y.; Hu, P.; Lee, M.-H.; Wang, H., Au on (111) and (110) surfaces of CeO2: A density-functional theory study. *Surf. Sci.* **2008,** *602* (10), 1736-1741.
4. Tang, Y.; Wei, Y.; Wang, Z.; Zhang, S.; Li, Y.; Nguyen, L.; Li, Y.; Zhou, Y.; Shen, W.; Tao, F. F.; Hu, P., Synergy of Single-Atom Ni1 and Ru1 Sites on CeO2 for Dry Reforming of CH4. *J. Am. Chem. Soc.* **2019,** *141* (18), 7283-7293.
5. Song, W.; Su, Y.; Hensen, E. J. M., A DFT Study of CO Oxidation at the Pd–CeO2(110) Interface. *J. Phys. Chem. C* **2015,** *119* (49), 27505-27511.
6. Tian, D.; Zeng, C.; Wang, H.; Cheng, X.; Zheng, Y.; Xiang, C.; Wei, Y.; Li, K.; Zhu, X., Effect of transition metal Fe adsorption on CeO2 (110) surface in the methane activation and oxygen vacancy formation: A density functional theory study. *Appl. Surf. Sci.* **2017,** *416*, 547-564.
7. Cui, L.; Tang, Y.; Zhang, H.; Hector, L. G.; Ouyang, C.; Shi, S.; Li, H.; Chen, L., First-principles investigation of transition metal atom M (M = Cu, Ag, Au) adsorption on CeO2(110). *Phys. Chem. Chem. Phys.* **2012,** *14* (6), 1923.
8. Tang, Y.; Asokan, C.; Xu, M.; Graham, G. W.; Pan, X.; Christopher, P.; Li, J.; Sautet, P., Rh single atoms on TiO_2 dynamically respond to reaction conditions by adapting their site. *Nat. Comm.* **2019,** *10* (1), 4488.